

Evolutionary Dynamics on Scale-Free Interaction Networks

Joshua L. Payne, *Student Member, IEEE* and Margaret J. Eppstein

Abstract—There has been a recent surge of interest in studying dynamical processes, including evolutionary optimization, on scale-free topologies. While various scaling parameters and assortativities have been observed in natural scale-free interaction networks, most previous studies of dynamics on scale-free graphs have employed a graph-generating algorithm that yields a topology with an uncorrelated degree distribution and a fixed scaling parameter. In this paper, we advance the understanding of selective pressure in scale-free networks by systematically investigating takeover times under local uniform selection in scale-free topologies with varying scaling exponents, assortativities, average degrees, and numbers of vertices. We demonstrate why the so-called characteristic path length of a graph is a nonlinear function of both scaling and assortativity. Neither the eigenvalues of the adjacency matrix nor the effective population size was sufficient to account for the variance in takeover times over the parameter space that was explored. Rather, we show that 97% of the variance of logarithmically transformed average takeover times, on all scale-free graphs tested, could be accounted for by a planar function of: 1) the average inverse degree (which captures the effects of scaling) and 2) the logarithm of the population size. Additionally, we show that at low scaling exponents, increasingly *positive* assortativities increased the variability between experiments on different random graph instances, while increasingly *negative* assortativities increased the variability between takeover times from different initial conditions on the same graph instances. We explore the mechanisms behind our sometimes counterintuitive findings, and discuss potential implications for evolutionary computation and other relevant disciplines.

Index Terms—Assortativity, complex networks, interaction networks, interaction topologies, invasion dynamics, population structure, saturation dynamics, scale-free, takeover time analysis.

I. INTRODUCTION

THE BEHAVIOR of a complex adaptive system is governed by the collective dynamics of its interacting system components. Consequently, the topological characteristics of the interaction network that specifies which components can interact with one another have a pronounced influence on the rate of information flow throughout the system, and thus play a critical role in determining emergent system-wide dynamics. For example, the evolution of altruism [1] and

cooperation [2]–[5], species invasiveness [6], disease propagation [7]–[9], energy transfer in food webs [10], predator-prey dynamics [11], the maintenance of genetic diversity [12]–[14], the suppression of evolutionary pathologies [15], and the self-organization of barriers to gene flow [16] have all been shown to be highly dependent on the topological properties of the underlying interaction network.

In the context of evolutionary computation, interaction networks are often utilized as population structures. This was initiated in the design of parallel evolutionary algorithms (for a review of this topic, see [17]), where populations are typically structured into subpopulations that are distributed onto separate processing units. Mating interactions are usually panmictic within the subpopulations, with periodic migration occurring between subpopulations according to an explicit subpopulation interaction topology (e.g., all-to-all, grid-based, etc.) [18]–[23]. While population structures can thus be exploited for computational efficiency of parallel implementations of evolutionary algorithms, there has also been an increasing interest in exploiting different population structures to improve the effectiveness of evolutionary search. In cellular evolutionary algorithms, populations are structured on low-order regular graphs, such as a 1-D or 2-D lattice, and mating events are restricted to occur within spatially localized overlapping neighborhoods. In these regular population structures, the imposition of spatial constraints on recombination events has been shown to improve the maintenance of genetic diversity, in part by retarding the flow of advantageous alleles and consequently reducing the selective pressure [24]. While 1-D and 2-D lattice population structures are the most commonly used interaction networks for evolutionary optimization, the utilization of other regular graph structures, such as the generalized Peterson graph and the complete bipartite graph, have recently been investigated as well [25], wherein the performance improvements obtained on each graph structure were shown to be problem dependent.

In contrast to these regular population structures, the interaction networks of numerous natural populations have been found to be heterogeneous (i.e., different nodes in the interaction network have different numbers of connections). Of particular interest are scale-free networks [26], a class of highly heterogeneous graphs, which have been shown to be quite ubiquitous in natural systems, ranging from networks of social interactions, such as email networks [27] and sexual contacts [28], to cellular systems, such as metabolic networks [29], [30] and protein–protein interactions [31]. Accordingly, there has been a recent surge of interest in studying dynamical

Manuscript received September 29, 2008; revised January 19, 2009; accepted March 15, 2009. First version published July 28, 2009; current version published August 14, 2009. This paper was funded in part by Vermont EPSCoR (NSF EPS 0701410) through a Graduate Research Fellowship awarded to J. L. Payne and a Pilot Project Award granted to M. J. Eppstein.

The authors are with the Department of Computer Science, University of Vermont, Burlington, VT 05405 USA (e-mail: Joshua.Payne@uvm.edu; Maggie.Eppstein@uvm.edu).

Digital Object Identifier 10.1109/TEVC.2009.2019825

processes on scale-free topologies; examples include the saturation dynamics of infectious disease in epidemiological models [8], information cascades in binary decision models [32], the emergence of cooperative behavior in evolutionary games [4], [33], [34], and evolutionary optimization [35]–[38]. In particular, scale-free population structures have been analyzed in the context of genetic algorithms with self-adaptive mutation [36] and multiobjective optimization [37], [38], and have been applied to the localization problem in robotics [35], with each study demonstrating varying degrees of success. For example, while Giacobini *et al.* [36] found that populations evolving on scale-free topologies were unable to outperform panmictic populations on a variety of benchmark optimization problems, Gasparri *et al.* [35] found that scale-free population structures enhanced the genetic algorithm's ability to solve both the localization and kidnap problems in a mobile robotics application. Such mixed results were also reported by Kirley and Stewart [37], [38]. While populations evolving on scale-free topologies were outperformed by populations evolving on random topologies on a two-objective problem (in terms of convergence speed and spread of solutions across the Pareto front) [37], populations evolving on scale-free population structures were shown to outperform populations evolving on random, small-world [39], and regular lattice population structures as the number of objectives increased, on specific multiobjective problems [38].

Scale-free topologies exhibit a power-law distribution of vertex connectivity, such that the probability $p(k)$ of having a vertex of degree k is of the form $p(k) \propto k^{-\gamma}$, where γ is referred to as the scaling parameter. Various scaling exponents have been measured in natural systems, e.g., $\gamma \sim 2.4$ for the number of species per genus of mammals and $\gamma \sim 3.1$ for the protein–protein interaction network of *S. cerevisiae* [40]. The propensity with which vertices of similar degree (i.e., number of connections) are connected to one another is referred to as the assortativity (r) of the network [41]. Some scale-free interaction networks (e.g., societal interactions) exhibit “positive assortativity” [41], where vertices of high degree are more likely to be connected to one another than to vertices of low degree. Other scale-free networks (e.g., protein–protein interactions), exhibit “negative assortativity” [41], where nodes of high degree are more likely to connect to nodes of low degree. Networks in which there is no relationship between the degree of adjacent vertices, such as those produced by the preferential attachment algorithm provided by Albert and Barabási (AB) [26], are referred to as “uncorrelated.”

While various scaling parameters and assortativities have been observed in natural systems, most previous studies of dynamics on scale-free graphs (including the evolutionary optimization studies cited above) were generated using the AB algorithm, which yields uncorrelated topologies ($r \sim 0$) [41] with a scaling parameter that approaches $\gamma \sim 3$ [26], as the number of vertices approaches infinity. However, a few recent studies have shown that both scaling and assortativity exert important influences on graph-based dynamical processes. For example, the equilibrium proportion of cooperators in the prisoner's dilemma played on scale-free networks has been

shown to decrease as the scaling exponent γ increases [33], or as the assortativity deviates from an uncorrelated mixing pattern ($r \neq 0$) [34]. In the unbiased Voter Model, recent results [42] have demonstrated that the expected consensus time on scale-free graphs increases as the scaling exponent increases, and that assortativity has a smaller secondary effect on the amount of time required to reach consensus.

In order to better understand the potential for evolutionary optimization on scale-free graphs, it is important to understand how both scaling and assortativity affect fundamental system dynamics. Such an understanding may also provide insight into other types of dynamic processes on scale-free networks, including spread of infectious disease and dissemination of fads and ideas.

One commonly employed method for quantifying selective pressure in evolutionary algorithms is through the analysis of the dynamics with which a single favorable mutation spreads throughout the population (aka “takeover time analysis”) [43]. Higher takeover times imply lower selective pressure, and vice versa. Takeover times have been previously investigated and modeled in several regular population structures. Goldberg *et al.* [43] investigated saturation dynamics in panmictic population structures (i.e., complete graphs) under a variety of selection mechanisms and showed that takeover is quite rapid in such well-mixed systems. Rudolph [44] provided exact analytical solutions for expected saturation times on ring structures (i.e., 1-D toroidal lattice) and lower and upper bounds for array structures (i.e., 1-D non toroidal lattice). Sarma and De Jong [45] investigated takeover times in 2-D toroidal lattices with neighborhoods of various shapes and sizes and showed that selective pressure is largely governed by the radius of the local mating neighborhood, and Giacobini *et al.* [24] provided mathematical models of takeover dynamics in 1-D and 2-D (with Von Neumann neighborhoods) toroidal lattices using synchronous and asynchronous updating policies.

Analysis of takeover times in irregular population structures has received considerably less attention. Giacobini *et al.* [46] provided analytical approximations of takeover dynamics in random graphs and empirical results for small-world topologies [39]. Their results demonstrated that random graphs induce a selective pressure qualitatively similar to panmixia and that the selective pressures induced by small-world topologies approach that of a random graph as the probability of creating long-distance interactions increases. In the same study [46], they showed that the average selective pressures induced by the AB scale-free population structures they employed were at least as strong as those induced by random graphs and that, when the initial copy of the high-fitness individual was strategically placed in a highly connected vertex of an AB graph, takeover was even faster than with panmixia.

In a preliminary study [47], we measured takeover times using a variety of scale-free graph generating algorithms [26], [30], [48] with various degrees of clustering, modularity, and hierarchical organization (which resulted in a variety of scaling exponents and assortativities, although these parameters were neither systematically varied nor explicitly reported there). We showed that selective pressures on different types of

scale-free graphs vary from very high levels, comparable to those induced by random mixing, to very low levels that are even weaker than those induced by nearest neighbor interactions (Moore neighborhoods). In a follow-up study, we investigated the independent and combined influence of scaling (γ) and assortativity (r) on takeover times in scale-free topologies at a single population size, with fixed average degree [49]. In that work, we found that takeover times exhibited a nonlinear negative correlation with the scaling exponent and a nonlinear positive correlation with assortativity, with additional nonlinear interactions between these two topological properties. Further, we showed that with low scaling and high positive assortativity, takeover times were much less dependent on the degree of initial placement than on uncorrelated [46], [49] and negatively assortative [49] scale-free graphs.

Ideally, expected takeover times in arbitrary population structures (regular or irregular) could be simply predicted using readily pre-computable metrics of the underlying interaction network. In related application domains, such as statistical physics and ecology, simple functional relationships have been determined between the structural properties of the interaction networks and the dynamic properties of spreading behavior. For example, consensus time in the unbiased Voter Model has recently been shown to be a function of the population size and the first and second moments of the degree distribution [42]. Investigations in heterogeneous ecological networks have shown that *indirect* pathways are an important governing influence in graph-based dynamical processes [10], [50]. Specifically, the leading eigenvalue of the network adjacency matrix has been shown to be a good measure of the rate with which the number of paths between vertices grows as a function of path length [50], and this has been shown to have a pronounced influence on the rate of flow of matter and energy throughout ecosystems [10]. In the context of evolutionary computation, the expected takeover time on regular graphs is known to be a positively correlated linear function of the characteristic path length [44], [47], a metric which quantifies the mean shortest distance between all pairs of vertices. In addition, we have recently shown that differential equation-based analytical methods, based on pair approximations, can be parameterized by the ratio of the local neighborhood radius to the global lattice radius in order to rapidly estimate pre-equilibrium takeover dynamics in grid-based regular population structures [51]. The problem has proved more elusive in the case of scale-free topologies with stochastic degree-dependent update policies. In [47], we suggested that average takeover times on scale-free topologies were positively linearly correlated with a combination of the maximum and variance of the all-pairs shortest path lengths. However, our subsequent work [49] showed that takeover times were actually a logarithmic function of the metric presented in [47] in uncorrelated and positively assortative scale-free graphs, with the slopes varying as a function of assortativity, while takeover times in negatively assortative scale-free graphs were completely independent of this metric. Conversely, while average takeover time was shown to be an ambiguous multifunction of the characteristic path length in uncorrelated and positively assortative scale-free graphs,

characteristic path length was found to have a *negative* non-linear correlation with takeover times in negatively assortative scale-free graphs (a counterintuitive result, given that this correlation is *positive* in regular graphs).

The results of our previous studies thus indicate that metrics based on all-pairs shortest direct paths are not sufficient to explain the rate of information flow in scale-free networks with stochastic, degree-dependent update policies. In this paper, we seek to understand why this observation is true and to determine if there are other static network properties that govern takeover times on scale-free topologies with varying scaling exponents, assortativities, average degrees, and population sizes (i.e., number of vertices). We significantly extend our previous studies [47], [49] on takeover times under local uniform selection in scale-free interaction networks. In Section II, we explain how we generated and employed scale-free graphs with systematically varying scaling exponents, assortativities, average degrees, and population sizes. In Section III we show *why* characteristic path length is a nonlinear non-monotonic function of both scaling and assortativity, and thus does not govern takeover time. We demonstrate that the influence of scaling and assortativity on average takeover times is qualitatively similar under three different stochastic selection mechanisms: uniform selection, binary tournament selection, and linear ranking selection. We then show that the logarithm of average takeover times in scale-free topologies can be described as a planar function of the average inverse degree and the logarithm of population size, and that assortativity exerts a strong influence on the variability in takeover times at low scaling exponents. In Section IV, we discuss our findings and their relevance to other disciplines, and suggest ways in which the structural characteristics of scale-free interaction networks can potentially be exploited in evolutionary optimization.

II. METHODS

A. Representing Population Structure as a Graph

The population structure of an evolutionary algorithm can be represented as a graph $G = (V, E)$, defined as a nonempty finite set of vertices (V) and a finite set of edges (E) connecting these vertices. Each individual in the population is represented by a vertex $i \in V$, so that $|V| = N$, where N is the population size. The graph is undirected, with an edge $\langle i, j \rangle \in E$ for every individual j in the mating neighborhood of individual i , for all $i \in V$. The number of neighbors in the mating neighborhood of individual i , which is also referred to as the *degree* of vertex i , is denoted by k_i . Throughout this paper, the terms *population structure*, *topology*, *network*, and *graph* are used synonymously.

B. Structural Properties of Graphs

When quantifying the structural properties of graphs, there are several metrics of potential interest (e.g., see [52]). In this section, we present the topological properties considered in this paper (for the readers' convenience, we also present a glossary of variables in the Appendix). The distribution of vertex connectivity $p(k)$ is a probability distribution function

(PDF) that depicts the frequency with which a node has degree k . The scale-free topologies considered in this paper possess a distribution of vertex connectivity of the form

$$p(k) = \Pr(K = k) \propto k^{-\gamma}. \quad (1)$$

The complementary cumulative distribution function (CCDF), which is commonly used to visualize power-law distributions [40], depicts the frequency with which nodes have degree greater than or equal to k

$$p(k) = \Pr(K \geq k) \propto k^{-\gamma+1}. \quad (2)$$

In (1) and (2), the scaling parameter γ affects the shape of the power-law distribution, such that distributions with smaller γ possess heavier tails (Fig. 1).

The i th moment (μ_i) of the degree distribution is given by

$$\mu_i = \sum_k k^i p(k) \quad (3)$$

such that μ_1 is the average degree ($\langle k \rangle$) and μ_{-1} is the average inverse degree. It is important to point out that while the average degree (μ_1) is unaffected by changes in the scaling exponent (γ), the average inverse degree (μ_{-1}) changes as a function of both γ and $\langle k \rangle$. Since the graphs considered are connected, μ_{-1} is always well defined.

A path is defined as a sequence of vertex–edge pairs, beginning at one vertex i and ending at another vertex j ; the direct distance $\text{dist}(i, j)$ between any two nodes i and j is defined as the length of the shortest path between i and j . The average individual path length L_i of a vertex i is defined as the mean of the shortest paths between i and all other vertices in the graph

$$L_i = \frac{1}{|V| - 1} \sum_{j \neq i \in V} \text{dist}(i, j). \quad (4)$$

The characteristic path length L of a graph G is defined as the mean of the individual path lengths

$$L = \frac{1}{|V|} \sum_{i \in V} L_i. \quad (5)$$

The assortativity (r) of a graph G measures the propensity with which vertices of similar degree are connected to one another. Assortativity is formally defined as [41]

$$r = \frac{|E|^{-1} \sum_{\forall (i,j) \in E} k_i k_j - \left[|E|^{-1} \sum_{\forall (i,j) \in E} \frac{1}{2} (k_i + k_j) \right]^2}{|E|^{-1} \sum_{\forall (i,j) \in E} \frac{1}{2} (k_i^2 + k_j^2) - \left[|E|^{-1} \sum_{\forall (i,j) \in E} \frac{1}{2} (k_i + k_j) \right]^2} \quad (6)$$

which is equivalent to the Pearson correlation coefficient of the degrees of vertices at the opposing ends of an edge [41]. A graph is said to be *positively assortative* if $r > 0$, *uncorrelated* if $r = 0$, and *negatively assortative* if $r < 0$.

It is worth noting that the radius [45] of a local interaction neighborhood, which exhibits a strong effect on saturation

times in regular population structures [45], [51], is not a meaningful metric in the case of scale-free topologies, since these graphs are not embedded in Cartesian space.

C. Takeover Time Analysis

In order to most directly infer the influence of the structural properties of scale-free interaction networks on the saturation times of advantageous alleles, we minimized 1) the number of different alleles, and 2) the complexity of the selection operator. Specifically, we consider a population with only two levels of fitness (as in [24], [44], [47], [49], [51]); i.e., let $\Lambda_i(t)$ be the fitness value of vertex $i \in V$ at time t , where $\Lambda_i(t) \in \{0, 1\}$ and 1 is more fit than 0. In the initial population, $\Lambda_i(0) = 1$ for exactly one $i \in V$ and $\Lambda_j(0) = 0 \forall j \neq i \in V$. Let N_t denote the *proportion* of nodes with value 1 at time t

$$N_t = \frac{1}{|V|} \sum_{\forall i \in V} \Lambda_i(t). \quad (7)$$

Following [44], we define the takeover time $T = \min\{t | N_t = 1\}$ of an experiment to be the first generation in which the fittest genotype fully saturates the population, starting from a single copy of this genotype. This definition of takeover time thus assumes that N_t can never decrease.

$E_i[T]$ is defined as the empirical estimate of the expected takeover time given that the initial best individual is located in vertex i . Thus, the overall empirically estimated expected takeover time of a beneficial mutation, averaged over all potential initial conditions, is simply

$$E[T] = \frac{1}{|V|} \sum_{\forall i \in V} E_i[T] \quad (8)$$

assuming that the initial best individual is equally likely to appear in any given node.

We tested three stochastic selection mechanisms that have been used in previous takeover time analyses: local uniform selection [53], binary tournament selection [24], and linear ranking selection [24]. Note that in heterogeneous graphs with a minimum node degree of 2, tournaments of larger sizes are not possible for all nodes, and in takeover studies with only two levels of fitness, ranking is arbitrary within nodes of the same fitness level. Our tests verified that the influence of scaling and assortativity on takeover dynamics is qualitatively similar under these three selection mechanisms, (see Section III-B). Thus, consistent with previous studies of takeover dynamics on heterogeneous networks [46], [47], [49], the remainder of our experiments utilized local uniform selection [53], with a simple “replace if better” survivor selection mechanism, as described below.

Each node is updated synchronously, as follows: for each node $i \in V$, a node j is selected at random with uniform probability from the mating neighborhood of node i , with neighborhood size k_i . Thus, if there are x nodes containing the fittest value in the mating neighborhood of node i , then the probability of selecting one of them (P_{sel}) is simply

$$P_{\text{sel}} = \frac{x}{k_i}. \quad (9)$$

The value of node i is then replaced by the value of node j if j has higher fitness [i.e., $\Lambda_j(t) > \Lambda_i(t)$].

D. Generating Scale-Free Topologies with Tunable Scaling and Assortativity

Several methods have been proposed for generating topologies with power-law distributions of vertex connectivity (e.g., [54]–[56]). However, most of these graph-generating algorithms produce topologies that consist of a single giant connected component and several small clusters of vertices that are isolated from the rest of the graph, effectively resulting in an unnecessary reduction of the population size. Further, most scale-free graph generating algorithms produce topologies that asymptotically approach fixed structural properties (e.g., the AB algorithm produces graphs with γ approaching 3 and r approaching 0, as N approaches ∞). In this paper, we wanted to generate connected scale-free topologies that possess well-controlled scaling exponents and assortativities, but whose interconnections are otherwise random. In the following sections we describe the algorithms used to create these graphs.

1) *Tuning the Scaling Exponent:* In order to generate scale-free topologies with tunable scaling exponents, we utilized the growing network (GN) model of Krapivsky, Redner, and Leyvraz [57], which is a generalization of the AB algorithm. Each graph was initialized as a fully connected clique of m_0 nodes (whereas in original GN model [57] the graph is initialized with only one node). In each time step t , a single node is added to the graph and is connected to m existing nodes, such that the probability of connecting to an existing node of degree k is proportional to the linear connection kernel A_k

$$A_k = \begin{cases} m_0, & \text{if } k = m_0 \\ \alpha k, & \text{if } k > m_0. \end{cases} \quad (10)$$

The probability Π that a newly introduced vertex attaches to an existing vertex i of degree k_i is then given by

$$\Pi(k_i) = \frac{A_{k_i}}{\sum_{\forall j \in V} A_{k_j}}. \quad (11)$$

After t time steps, the graph consists of $m_0 + t$ vertices and $\binom{m_0}{2} + mt$ edges, where $t = N - m_0$. So long as $m = m_0$, graph connectivity is ensured, since the first incoming node is forced to connect to all m_0 nodes in the initial clique. Note that if $\alpha = 1$, the AB algorithm is recovered.

By tuning the parameter α in (10), the scaling exponent can be theoretically tuned anywhere in the range $2 < \gamma < \infty$, for infinitely sized graphs. (Graphs with $\gamma \leq 2$ possess degree distributions with infinite mean and variance.) While an analytical formulation of γ as a function of α is provided in [57], this formulation assumes that the graph is infinitely large, and can only be used as a rough approximation for the finite graphs considered herein. Thus, the values of α used in this paper to generate graphs with specific scaling exponents, at various population sizes and average degree, were determined empirically. Due to finite size effects and the stochastic nature of the GN algorithm, the mapping of α to γ is not one-to-one, and a range of scaling exponents (γ) will be observed for any given α . In order to generate a graph with a specific desired scaling exponent γ , a graph was

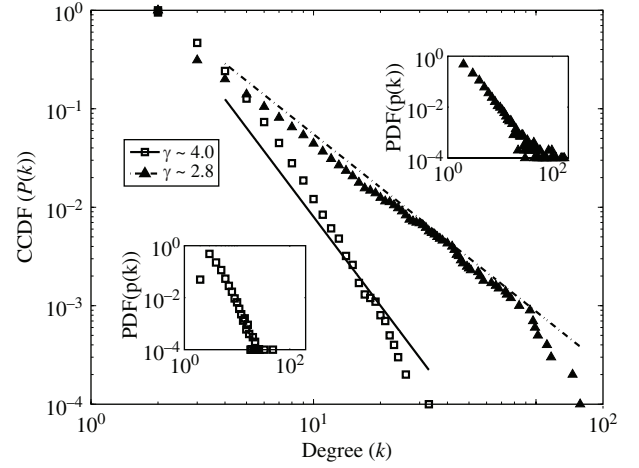


Fig. 1. Data points showing representative complementary cumulative distribution functions (CCDF) of vertex connectivity in randomized scale-free interaction networks created with the GN algorithm (Section II-D.1), with the smallest and largest scaling exponents used in this paper $\gamma \in \{2.8, 4.0\}$ and $\langle k \rangle = 4$. Lines are drawn using the scaling exponents measured using the algorithm described in Section II-D.2 with a k_{\min} of 4, and are deliberately offset in the vertical direction so as not to obscure the data. Data shown pertain to $N = 10,000$. Note the double logarithmic scale. Insets denote the corresponding probability distribution functions (PDF), showing how the observed frequency of occurrence is lower-bounded by $1/N$ in these finite-sized graphs.

generated using the empirically predetermined value of α , and the observed γ was then calculated for the graph (as described in the subsequent section). Only if the graph had the desired γ (to within 0.01), was it retained and included in the study.

2) *Measuring the Scaling Exponent:* Accurately estimating the scaling parameter (γ) of data that are thought to be drawn from a power-law degree distribution is an area of current research [40]. One common method for estimating γ is to use the slope of the best linear fit between $\log_{10}(p(k))$ and $\log_{10}(k)$. While this method is straightforward, it has been shown to introduce significant bias in common cases [40].

In order to avoid such bias, we estimated γ using the method provided by Clauset, Shalizi, and Newman [40]. This method systematically varies γ over a specified range and iteratively applies the Kolmogorov–Smirnov (KS) test to the observed data and fitted model. The γ that minimizes the KS statistic is then chosen as the hypothesized power-law model. The goodness of fit of this model is then calculated using a Monte Carlo procedure [40] in order to verify that the degree distribution is, in fact, drawn from the hypothesized power-law model. While the minimum degree (k_{\min}) of the hypothesized power-law model can be simultaneously estimated [40], in this paper it was sufficient to simply use $k_{\min} = \langle k \rangle$.

3) *Shuffling the Edge Set:* In order to eliminate any structural motifs that may have been inadvertently introduced into the topology as an artifact of the GN algorithm, we utilized the method provided by Maslov and Sneppen [58] to randomize the edge set of every topology used in this paper. The Maslov–Sneppen algorithm is an iterative method that, in each iteration, randomly chooses two edges, $\langle a, b \rangle$ and $\langle x, y \rangle$, from the edge set E (where a, b, x, y are all distinct). These edges are then shuffled to create two new edges $\langle a, x \rangle$ and $\langle b, y \rangle$, which

replace the original edges, so long as they are not already present in the graph. Since the degree of each vertex remains unchanged by a shuffling event, this method exactly preserves the underlying degree distribution.

4) *Tuning the Assortativity*: In order to investigate the relationship between various assortativities and saturation times in scale-free topologies, we devised a simple iterative method that allows for the direct specification of assortativity within some error tolerance, as follows. In each iteration of our algorithm, the assortativity of the graph is measured using (6) and compared to the desired assortativity. Two edges, $\langle a, b \rangle$ and $\langle x, y \rangle$, are randomly selected from the edge set E (where a, b, x, y are all distinct) with uniform probability. If the observed assortativity is less than the desired assortativity, the edges are swapped such that the two nodes with the larger degree are connected to one another and the two nodes with the smaller degree are connected together (a “positive” assortative swap). If the observed assortativity is greater than the desired assortativity, the reverse swap is done (a “negative” assortative swap). If either of the new edges is already present in the graph, then the swap is aborted. The algorithm iteratively continues swapping edges in this fashion until the observed assortativity is within 0.01 of the desired assortativity or until a specified maximum number of swaps is reached (in this paper, we set the maximum number of swaps to 1 000 000). Like the Maslov–Sneppen algorithm, this method exactly maintains the underlying degree distribution, since the degree of each node remains unchanged after a swapping event. Since neither our assortative shuffling algorithm nor the Maslov–Sneppen algorithm guarantees that the graph remains connected, we discarded graphs that became disconnected, as discussed in Section II-D.5, step 4.

Our algorithm is similar to the single-parameter shuffling algorithm proposed by Xulvi-Brunet and Sokolov [59], which probabilistically alternates between Maslov–Sneppen edge swaps and edge swaps that alter assortativity. However, the non-determinism in the selection of the edge-swapping algorithm results in a range of assortativities for a given specified probability, whereas our method enables us to more closely achieve the desired degree of assortativity (to within some small error tolerance), thus facilitating the generation of topologies with well-controlled assortativities.

Although assortativity can theoretically range from $-1 \leq r \leq 1$, in reality the actual range of assortativities in scale-free graphs that we were able to obtain, using the algorithms described above, was much more constrained. The positive (negative) assortativity limits were empirically assessed by performing 10 million positive (negative) assortative edge swaps on ten graph instances, for population sizes $N \in \{1000, 1600, 3600, 6400, 10000\}$, and $\gamma \in \{2.4, 2.8, 3.2, 3.6, 4.0\}$, with $\langle k \rangle = 4$ [Fig. 2(a)] and $\langle k \rangle = 8$ (the data for $\langle k \rangle = 8$ were very similar to those for $\langle k \rangle = 4$, so for clarity are not shown). Population size and number of edges had no detectable effects on the achievable ranges of assortativity; however, we observed greater constraints on achievable assortativities at lower scaling exponents (γ). A symmetric range of assortativities for each scaling exponent was implicitly limited by these constraints, and further experiments were

thus run using assortativities from $-0.2 \leq r \leq 0.2$, for $2.8 \leq \gamma \leq 4$, as shown by the shaded box in Fig. 2(a). This range spans to either side of $\gamma = 3$, below which the variance of the degree distribution is theoretically infinite (this is not possible for finite graphs, resulting in a degradation in the scale-free behavior at high k , as shown in Fig. 1 for $\gamma \sim 2.8$). Parameters within this range have been observed in natural systems (e.g., a recent analysis [40] of empirical power law distributions arising in a variety of systems provides statistical support for scaling exponents ranging from 1.7 to 4.3). We use a relatively small ($N = 500$) scale-free interaction network with $\gamma = 2.8$ and $\langle k \rangle = 4$ to graphically illustrate how the topology qualitatively differs at two extremes of the parameter range shown in Fig. 2(a), when the assortativity of the graph is reshuffled to have positive assortativity $r = 0.2$ [Fig. 2(b)] or negative assortativity $r = -0.2$ [Fig. 2(c)]. Note that the degree distributions of these two graphs are identical.

5) *Summary of Scale-Free Graph Generation*: For each desired scaling exponent γ , assortativity r , population size N , and average degree $\langle k \rangle$, we performed the following steps.

- Step 1:** A graph was created using the GN algorithm, as presented in Section II-D.1, with $m_0 = m$.
- Step 2:** The scaling exponent (γ) of the resulting graph was measured using the method presented in Section II-D.2, with the minimum degree (k_{\min}) at which the scaling behavior was assessed set to $\langle k \rangle$ (Fig. 1). If the absolute difference between the observed and desired γ was greater than 0.01, or if the goodness of fit of the hypothesized power law model was not satisfactory ($p < 0.1$, as calculated using the Monte Carlo method presented in [40]), then the graph was discarded and Step 1) was repeated.
- Step 3:** Once a graph was created with an acceptable scaling exponent, it was randomized by performing 100 000 Maslov–Sneppen edge swaps, as described in Section II-D.3. If the graph became disconnected due to a swapping event, the shuffled graph was discarded and Step 3) was repeated.
- Step 4:** The graph was then further shuffled to obtain the desired degree of assortativity (r), using the method presented in Section II-D.4, until the absolute difference between the observed and desired assortativity was less than 0.01. If the graph became disconnected due to a swapping event, the shuffled graph was discarded and Step 4) was repeated. If the graph could not be shuffled to have the desired assortativity within 1 000 000 swapping events, the graph was discarded and Step 1) was repeated.

Self loops were implicitly or explicitly precluded by all steps in graph generation.

E. Experimental Design

In this paper, population sizes of $N \in \{1000, 1600, 3600, 6400, 10000\}$ were considered with average degree $\langle k \rangle \in \{4, 8\}$ ($m = 2$ and $m = 4$, respectively), where the scaling exponent was varied between $2.8 \leq \gamma \leq 4.0$ in increments of

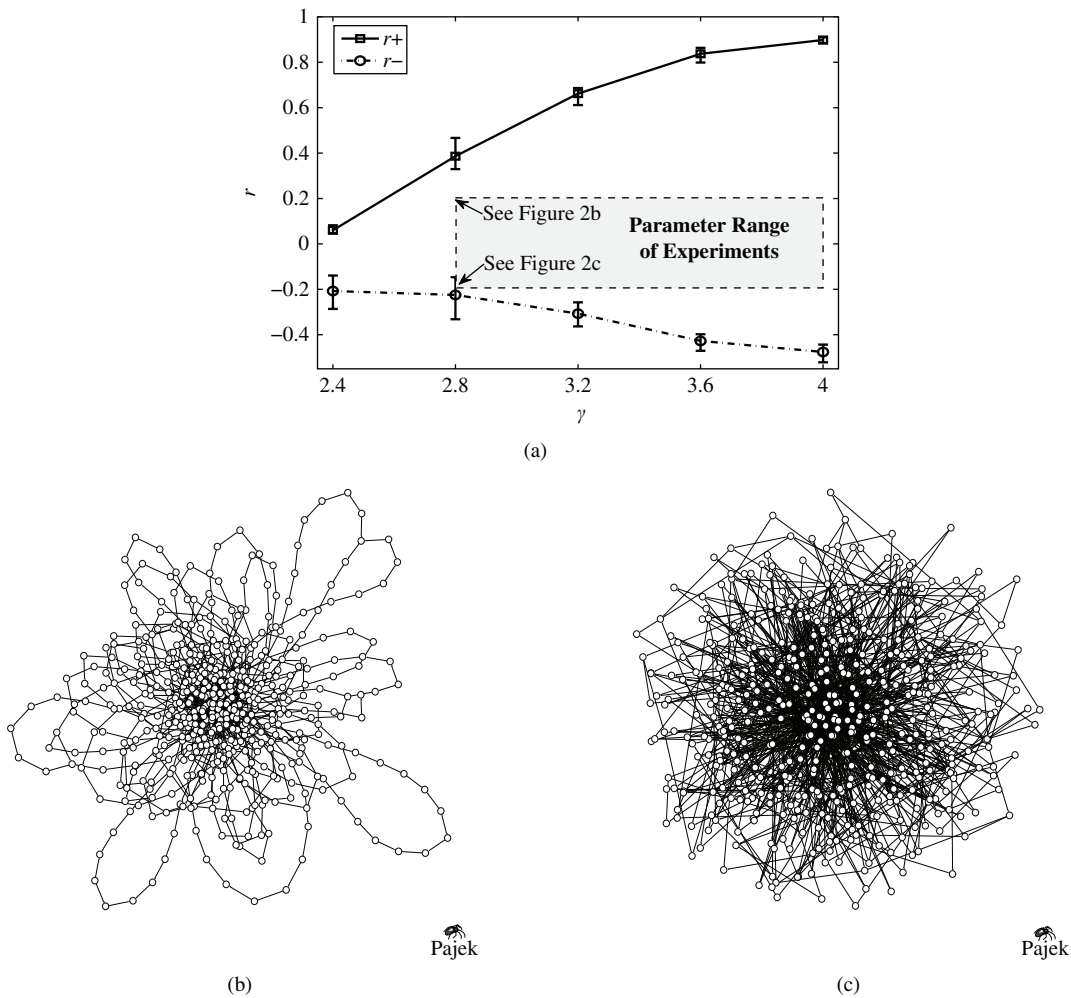


Fig. 2. (a) Upper bound of positive assortativities (r_+) and lower bound of negative assortativities (r_-) that we were able to obtain using the reshuffling algorithm described in Section II-D.4, as a function of the scaling parameter (γ). Data points are the averages of the maximum (or minimum) assortativities that were achieved in 10 million assortative edge swaps on each of ten graph instances at each of the five population sizes with $\langle k \rangle = 4$. Error bars indicate the minima and maxima observed for each combination of parameters. The shaded box indicates the range of experimental parameters examined in this paper. (b) Visualization of one representative positively assortative graph ($\gamma = 2.8$, $r = 0.2$, $N = 500$, $\langle k \rangle = 4$), and (c) visualization of one representative negatively assortative graph ($\gamma = 2.8$, $r = -0.2$, $N = 500$, $\langle k \rangle = 4$). In (b) and (c) the degree distribution of the graphs is identical. For visual clarity, the graphs shown in (b) and (c) are deliberately smaller than any used in the experiments; visualizations were made using Pajek [60].

0.4 and assortativity was varied between $-0.2 \leq r \leq 0.2$ in increments of 0.1. For each combination of N , $\langle k \rangle$, γ , and r , ten independent graph instances were generated by performing the steps detailed in Section II-D.5.

In contrast to regular population structures, the expected takeover times in scale-free interaction networks are known to be affected by the placement of the initial high fitness individual [46], [49]. Therefore, for each graph instance we systematically placed the high-fitness individual of the initial population in *each* vertex of the population structure, one at a time, and subsequently performed 10 independent takeover time simulations for each individual placement, in order to account for the stochasticity inherent in the selection mechanism. Thus, $100 \times N$ independent simulations were performed for each combination of N , $\langle k \rangle$, γ , and r , resulting in a total of over 140 million independent takeover time simulations.

To facilitate this extensive experimental design, simulations and graph generation were performed on a cluster of 128 dual-processor, dual-core (Opteron 2220) IBM x3455s,

each with 6 GB of memory. All of the graph-generating algorithms, edge-shuffling routines, and takeover simulations were written in the C programming language for speed. Data analysis was performed using MATLAB, as were the methods employed to measure scaling exponents, using the code provided with [40].

III. RESULTS

Results were qualitatively similar for all population sizes (N) and average degree ($\langle k \rangle$), so we initially present data for the representative population size of $N = 3600$ and $\langle k \rangle = 4$, and then show how the results scale as a function of population size and average degree. The first section pertains to the influence of scaling and assortativity on the static structural properties of the networks considered and the second section pertains to the dynamical properties of the takeover times observed on these networks.

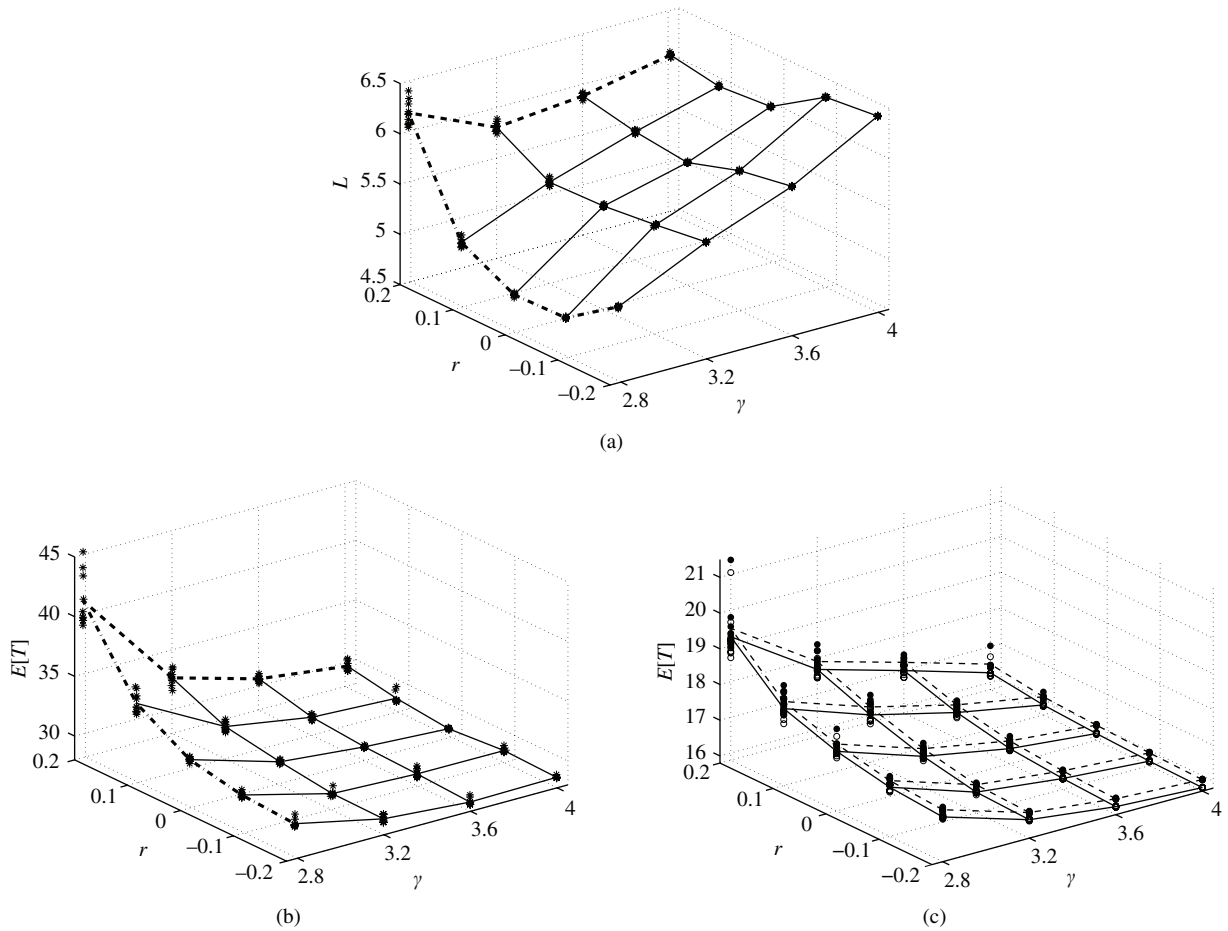


Fig. 3. (a) Characteristic path length (L) and (b) and (c) expected takeover time ($E[T]$), each shown as a surface function of assortativity (r) and scaling (γ) on a representative population size and average degree ($N = 3600$, $\langle k \rangle = 4$). The symbols represent the data points for each of the ten graph instances at each parameter combination, with lines connecting the means. Panel (b) corresponds to local uniform selection and (c) to binary tournament selection (\bullet symbols, dashed line) and linear ranking selection (\circ symbols, solid line). In (a) and (b) the dashed-dotted lines at $\gamma \sim 2.8$ correspond to the data presented in Figs. 5 and 6, and the dashed lines at $r \sim 0.2$ correspond to the data presented in Figs. 4 and 7.

A. Static Properties

Characteristic path length (L) was found to vary non-monotonically as a function of both the scaling exponent γ and assortativity r [Fig. 3(a)], consistent with the preliminary results presented in [49]. For $r \sim 0.2$ [Fig. 3(a), dashed line], L first decreases from $\gamma \sim 4.0$ to $\gamma \sim 3.2$ ($p \ll 0.01$, ANOVA) and subsequently increases from $\gamma \sim 3.2$ to $\gamma \sim 2.8$ ($p \ll 0.01$, ANOVA). Similarly, for $\gamma \sim 2.8$ [Fig. 3(a), dashed-dotted line], L is lowest at $r \sim 0$ and increases as the magnitude of assortativity (either positive or negative) increases. These nonlinear relationships between γ and L , and between r and L , result from changes in the distribution of underlying path lengths L_i , as described below.

Fig. 4 depicts the effect of decreasing the scaling exponent (γ) on the distribution of individual path lengths (L_i), and consequently on the characteristic path length (L), for a single representative graph instance with $N = 3600$, $\langle k \rangle = 4$, and $r \sim 0.2$ [this data corresponds to the dashed lines in Fig. 3(a) and (b)]. For $\gamma \sim 4.0$, the distribution of individual path lengths is approximately normally distributed ($p > 0.01$, χ^2 test) with a mean of $L = 6.05$ and standard deviation of 0.6 [Fig. 4(a)]. However, as γ decreases, the distribution

of path lengths deviates from normality ($p \ll 0.01$, χ^2 test) and begins to flatten and become increasingly skewed, with longer individual path lengths becoming more common as γ continues to decrease [(Fig. 4(b)–(d)]. For $\gamma \sim 3.6$ and $\gamma \sim 3.2$, the flattening of the distribution has the effect of decreasing L , but for $\gamma \sim 2.8$ the increase in the frequency of longer individual path lengths begins to play a dominating role, and L consequently increases (dashed vertical lines, $p \ll 0.01$, ANOVA).

Increasing the assortativity (r) has a similar impact on the underlying distribution of path lengths, and on the corresponding characteristic path length (L), as shown in Fig. 5, for a representative scale-free interaction network with $N = 3600$, $\langle k \rangle = 4$, and $\gamma \sim 2.8$. The path length distributions deviated from normality for all $\gamma \sim 2.8$ ($p \ll 0.01$, χ^2 test), though for $r \sim -0.2$, the path length distribution was found to be well centered around $L = 5.26$, with very few long paths [Fig. 5(a)]. However, for $r > 0.2$, the path length distribution was found to become increasingly flattened and skewed. Longer path lengths were found to occur more frequently as r increases, and their overall magnitude was found to increase [e.g., compare the horizontal spread of $*$ symbols in Fig. 5(a)]

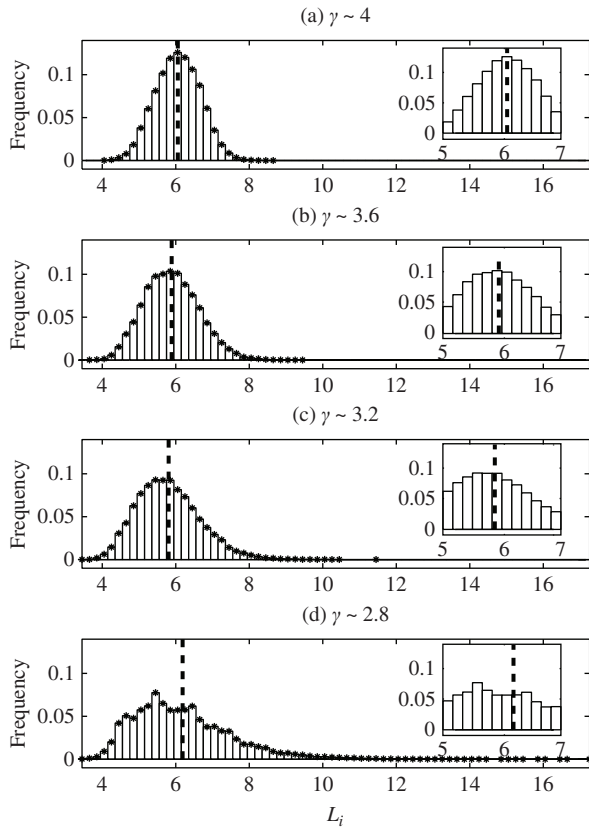


Fig. 4. Distribution of individual path lengths (L_i) in representative networks with $N = 3600$, $\langle k \rangle = 4$, and $r = 0.2$ for (a) $\gamma \sim 4$, (b) $\gamma \sim 3.6$, (c) $\gamma \sim 3.2$, and (d) $\gamma \sim 2.8$. The * symbols are placed atop each bin as a visual aid. The insets magnify the domain immediately surrounding the average characteristic path lengths L of the ten graph instances (denoted by the thick dashed vertical lines) in order to illustrate the nonlinear relationship between L and γ . Note that the data in this Figure corresponds to the data along the dashed line in Fig. 3(a).

with those in Fig. 5(e)]. Similar to the effect of decreasing γ , increasing r initially has the effect of decreasing L [dashed-dotted vertical lines for $-0.2 \leq r \leq 0$, $p \ll 0.01$, ANOVA, Fig. 5(a)–(c)], but as the frequency of longer path lengths and their overall magnitude increases, L subsequently begins to increase [dashed-dotted vertical lines for $0 < r \leq 0.2$, $p \ll 0.01$, ANOVA, Fig. 5(d) and (e)]. These changes in topology as a function of assortativity are graphically illustrated by comparing Fig. 2(b) (for positive assortativity), where there is a preponderance of long paths through vertices of degree $k = 2$, and Fig. 2(c) (for negative assortativity), where individual paths tend to alternate between high and low degree nodes, and are consequently more homogeneous in length.

B. Dynamic Properties

While characteristic path length (L) varied non-monotonically with both the scaling exponent (γ) and assortativity (r), [Fig. 3(a)], expected takeover times increased monotonically: 1) as assortativity was increased from $r \sim -0.2$ to $r \sim 0.2$ and 2) as the scaling exponent was decreased from $\gamma \sim 4.0$ to $\gamma \sim 2.8$ [Fig. 3(b) and (c)], for all three selection mechanisms considered. The variability in the average takeover times, for each of the ten graph instances at

each parameter combination, also increased with increasing r and decreasing γ [in Fig. 3(b) and (c), each *, •, and ○ symbol represents data points for the ten graph instances at each combination of r and γ].

The takeover times observed using binary tournament selection [Fig. 3(c), • symbols, dashed line] and linear ranking selection [Fig. 3(c), ○ symbols, solid line] were shorter than those observed under local uniform selection [Fig. 3(b)], because both of these selection mechanisms increase the probability of selecting high-fitness nodes from the local neighborhood, relative to uniform selection. However, the qualitative influence of scaling and assortativity on average takeover times was similar under all three selection mechanisms [compare Fig. 3(b) and (c)]. The remainder of our results were achieved using local uniform selection.

In Fig. 6, we depict the actual takeover dynamics [Fig. 6(a), (c), and (e)], and corresponding distributions of takeover times [Fig. 6(b), (d), and (f)], observed on a single representative scale-free interaction network with $N = 3600$, $\langle k \rangle = 4$, and $\gamma \sim 2.8$ [corresponding to the data around the dashed-dotted lines in Fig. 3(a) and (b)]. Fig. 3(b) indicates that both expected takeover times, and the variability in the expected takeover times *between graph instances*, increase with *increasing* assortativity. In contrast, Fig. 6 shows that the variability in takeover times *on a single graph instance*, due to different initial placements of the high fitness individual, actually *increases* with *decreasing* assortativity, while the average takeover time simultaneously *decreases* [e.g., at $\gamma \sim 2.8$ and $r \sim 0.2$, $E[T] = 43.2$, but this falls to $E[T] = 31.3$ at $r \sim -0.2$, Fig. 3(b)]. This occurs because, in negatively assortative graphs, some initial placements result in an extended initial period in which the high fitness genotype is unable to spread [compare Fig. 6(a), (c), and (e), gray lines], but a larger proportion of takeover times are comparatively more rapid than at high assortativity [compare the heights and locations of the peaks of the distributions in Fig. 6(b), (d), and (f)]. None of the distributions in Fig. 6(b), (d), and (f) is normal ($p \ll 0.01$, χ^2 test).

In contrast, decreasing the scaling exponent (γ) of a scale-free interaction network increases *both* the range and average of takeover times observed on a single graph instance, as shown for a representative topology with $N = 3600$, $\langle k \rangle = 4$, and $r \sim 0.2$ in Fig. 7 [corresponding to the data around the dashed lines in Fig. 3(a) and (b)]. In this case, the distribution of observed takeover times is shifted to the right and broadened as the scaling exponent decreases, with the expected takeover time increasing from $E[T] = 29.5$ (for $\gamma \sim 4.0$) to $E[T] = 43.2$ (for $\gamma \sim 2.8$), as shown in Fig. 7(b), (d), (f), and (h). Once again, none of the distributions of takeover times are normal ($p \ll 0.01$, χ^2 test).

We now shift our attention to how our results scale with population size (N) and average degree ($\langle k \rangle$). Since expected takeover time is an ambiguous multifunction of the characteristic path length, L cannot be used to describe takeover times (or selective pressure) in populations evolving on scale-free topologies. We also found that the leading eigenvalue of the network adjacency matrix is not a good indicator of takeover times in the general case. For the scale-free graphs

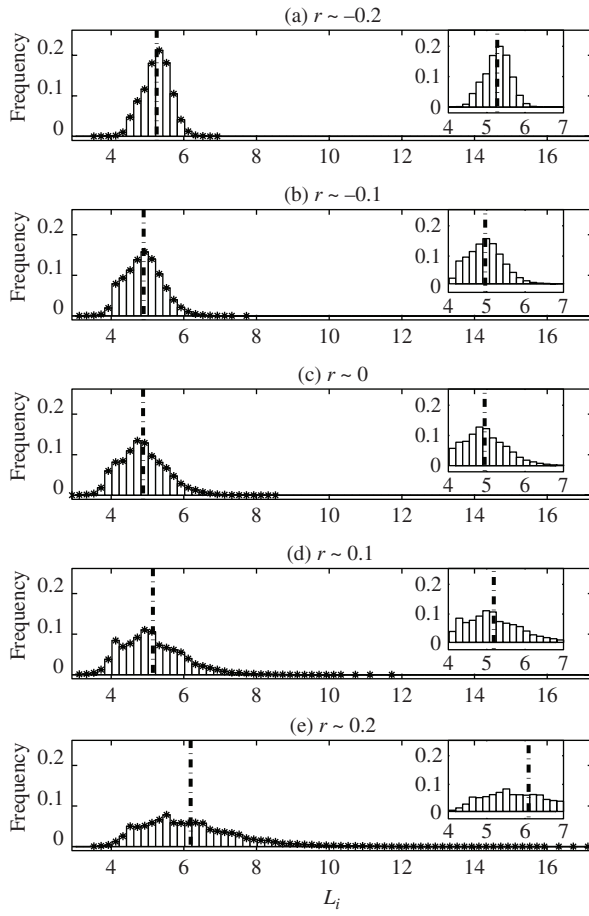


Fig. 5. Distribution of individual path lengths (L_i) in representative networks with $N = 3600$, $\langle k \rangle = 4$, and $\gamma \sim 2.8$ for (a) $r \sim -0.2$, (b) $r \sim -0.1$, (c) $r \sim 0$, (d) $r \sim 0.1$, and (e) $r \sim 0.2$. The * symbols are placed atop each bin as a visual aid. The insets magnify the domain immediately surrounding the average characteristic path lengths L of the ten graph instances (denoted by the thick dashed-dotted vertical line) in order to illustrate the nonlinear relationship between L and r . Note that the data in this Figure corresponds to the data along the dashed-dotted line in Fig. 3(a).

considered herein with $\langle k \rangle = 4$, the expected takeover time $E[T]$ was found to grow linearly in the leading eigenvalue of the adjacency matrix, for a given population size ($R^2 > 0.86$). However, this relationship was found to deteriorate as the average degree was increased to $\langle k \rangle = 8$ ($R^2 > 0.51$). Further, both the slope and intercept of the linear relationship between the leading eigenvalue and expected takeover time were found to differ between $\langle k \rangle = 4$ and $\langle k \rangle = 8$, with a combined R^2 of only 0.02. In contrast, for each population size N , we found that $E[T]$ increased exponentially in the average inverse degree (μ_{-1}) (with the goodness-of-fit $R^2 > 0.95$ for each N considered in this paper); note that (μ_{-1}) varies with *both* $\langle k \rangle$ and scaling exponent γ . Further, for both values of $\langle k \rangle$ considered, we found that the logarithm of the expected takeover time ($\log_{10}(E[T])$) scaled linearly with the logarithm of the population size ($\log_{10}(N)$) (the goodness-of-fit $R^2 = 0.70$ for $\langle k \rangle = 4$ and $R^2 = 0.87$ for $\langle k \rangle = 8$), with coefficients on $\log_{10}(N)$ less than 1, implying that $E[T]$ grows sub-linearly in N . Consequently, we constructed a 2-D best-fit function [depicted in Fig. 8(a)], which accurately describes

expected takeover time according to the following relationship:

$$\log_{10}(E[T]) = 0.80 + 0.11 \log_{10}(N) + 0.88 \mu_{-1} \quad (12)$$

with $R^2 = 0.97$ and a root mean squared error of only 1.32 between this plane and all of the data points (i.e., for all scaling exponents γ , assortativities r , average degrees $\langle k \rangle$, and population sizes N of the scale-free graphs considered herein). In Fig. 8(b), the viewing angle has been rotated to show the quality of the linear fit as a function of the average inverse degree μ_{-1} ; note that the differences in expected takeover time at each given average degree $\langle k \rangle$ and population size (N) are due to the effects of different scaling exponents (γ), which are captured by the average inverse degree (μ_{-1}). In Fig. 8(c), the viewing angle has been rotated to show the quality of the linear fit as a function of $\log_{10}(N)$.

Much of the heteroskedasticity in $E[T]$ as a function of μ_{-1} , as evident in Fig. 8(b), is attributable to the effect of assortativity (r) on the variability in takeover times. Assortativity has a relatively small effect on the *average* takeover time $E[T]$, that is not modeled by (12). However, assortativity does have a strong influence on the *variability* of $E[T]$, particularly for scale-free graphs with low scaling exponents [e.g., compare the spread of the data points in Fig. 3(b) at $r \sim 0.2$ for $\gamma \sim 2.8$ and $\gamma \sim 4.0$]. In Fig. 9(a), we explicitly plot the standard deviations of average takeover times ($\sigma_{E[T]}$) as a surface function of r and γ , on the largest population size ($N = 10000$) with the smallest average degree ($\langle k \rangle = 4$), where this influence is most pronounced; i.e., these indicate the variabilities in the mean takeover times *between the 10 graph instances at each parameter combination* (already averaged over each of the N initial placements, which are already averaged over each of the ten repetitions at each initial placement). The $\sigma_{E[T]}$ increases nonlinearly as assortativity increases and scaling decreases and contributes to the variable spread of the data points around the plane in Fig. 8.

As previously noted, assortativity has the opposite effect on the variability in individual takeover times due to *different initial locations of the high fitness value in a single graph instance* (e.g., Fig. 6). This is explicitly shown in Fig. 9(b), where we plot σ_T (i.e., the standard deviations in individual takeover times T due to the N initial placements, which are already averaged over the ten repetitions at each initial placement, on each given graph instance) as a surface function of r and γ , again on the largest population size ($N = 10000$) with the smallest average degree ($\langle k \rangle = 4$), where this influence is most pronounced.

The same general relationships shown in Fig. 9(a) and (b) occur at lower population sizes and higher average degree, but are less pronounced because the magnitude of the variability in takeover times decreases with both of these parameters [Fig. 8]. Note that the scale of the y-axis is an order of magnitude lower for the variability in the mean takeover times observed on the ten different graph instances [Fig. 9(a)] than for the variability caused by the N different initial placements [Fig. 9(b)] at each parameter setting.

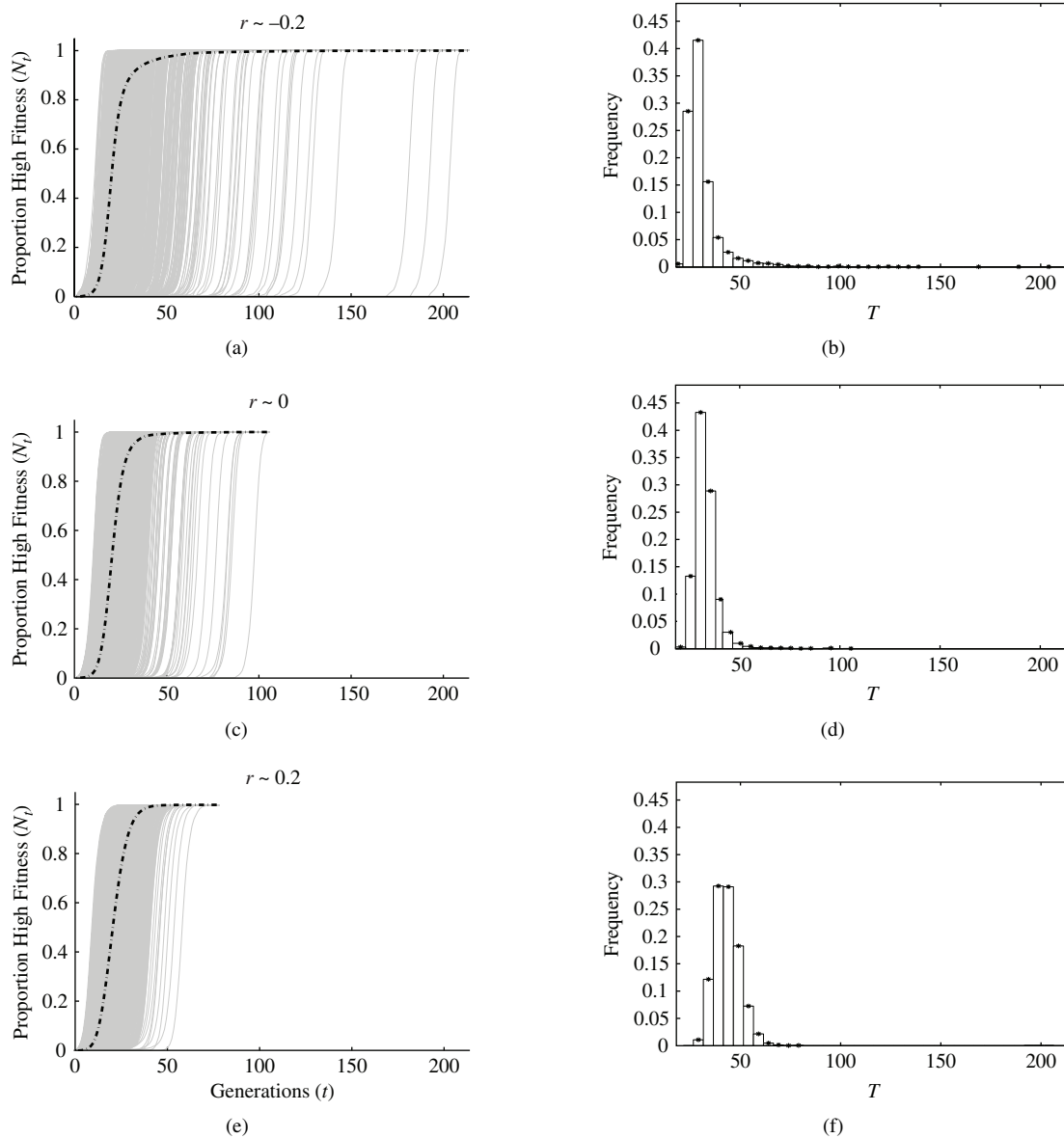


Fig. 6. Takeover dynamics in representative networks with $N = 3600$, $\langle k \rangle = 4$, and $\gamma \sim 2.8$ for (a) $r \sim -0.2$, (c) $r \sim 0$, and (e) $r \sim 0.2$ (corresponding to the dashed-dotted lines in Fig. 3(b)). The gray curves denote takeover dynamics for a single experiment and the dashed-dotted curves denote their averages. In (b), (d), and (f) we show frequency histograms of observed takeover times (T) for the data shown in (a), (c), and (e), respectively. The * symbols are placed atop each bin as a visual aid.

IV. DISCUSSION

The results of this paper demonstrate that in scale-free interaction networks with randomized edge sets, takeover time ($E[T]$) under local uniform selection increases as either: 1) the assortativity r increases or 2) the scaling exponent γ decreases, with these two topological properties interacting nonlinearly in their effect on takeover time [Fig. 3(b)]. In negatively assortative graphs ($r < 0$), nodes with high degree (aka “hubs”) are attached to nodes with low degree, and vice versa [Fig. 2(c)]. As such, placing the initial high fitness genotype in a hub results in rapid saturation, because the neighbors of a hub have few connections themselves and thus have a high probability of adopting the hub’s genetic information quickly. In contrast, placing the initial high-fitness genotype in a low-degree vertex that neighbors a hub can

result in a severe retardation of the propagation of this genetic information [Fig. 6(a)], because the hub has more neighbors to choose from. For example, if the initial high-fitness genotype is placed in a low-degree neighbor of a hub with degree k , then it will take on average k generations for this hub to adopt this high-fitness information, under the local uniform selection method outlined in Section II-C. While this has the effect of increasing the variability in the takeover times observed on a single graph instance [Fig. 6(a)], the extremely rapid saturation that occurs when the initial high-fitness genotype is placed in a highly connected node outweighs such occasional slow takeover time events, and causes an overall decrease in $E[T]$ as r decreases [Fig. 3(b)]. In positively assortative graphs ($r > 0$), hubs are connected to hubs, and nodes of low degree are connected to one another. For example, when

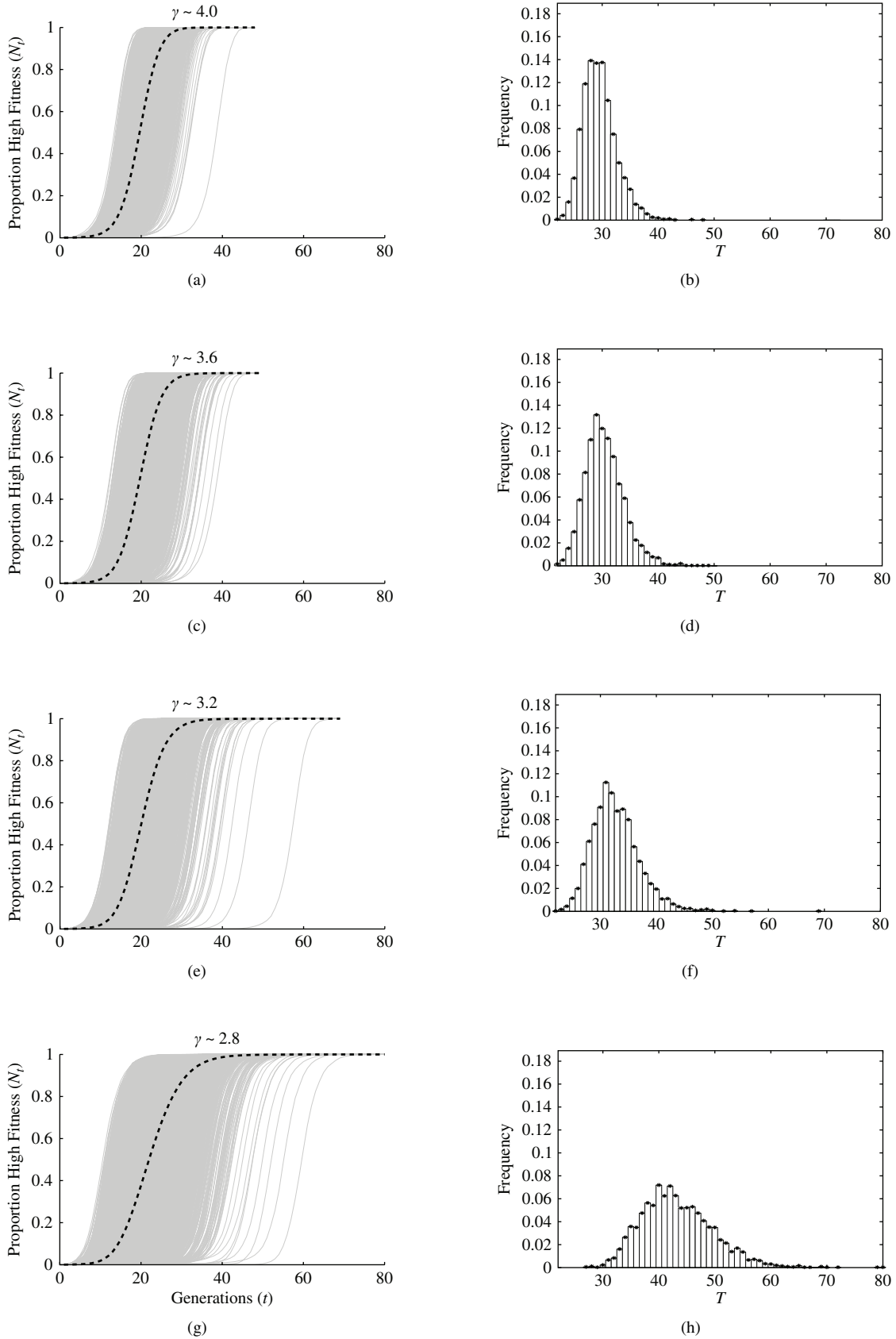


Fig. 7. Takeover dynamics in representative networks with $N = 3600$, $\langle k \rangle = 4$, and $r \sim 0.2$ for (a) $\gamma \sim 4.0$, (c) $\gamma \sim 3.6$, (e) $\gamma \sim 3.2$, and (g) $\gamma \sim 2.8$ (corresponding to the dotted lines in Fig. 3(b)). The gray curves denote takeover dynamics for a single experiment and the dashed curves denote their averages. In (b), (d), (f), and (h), we show frequency histograms of observed takeover times (T) for the data shown in (a), (c), (e), and (g), respectively. The * symbols are placed atop each bin as a visual aid.

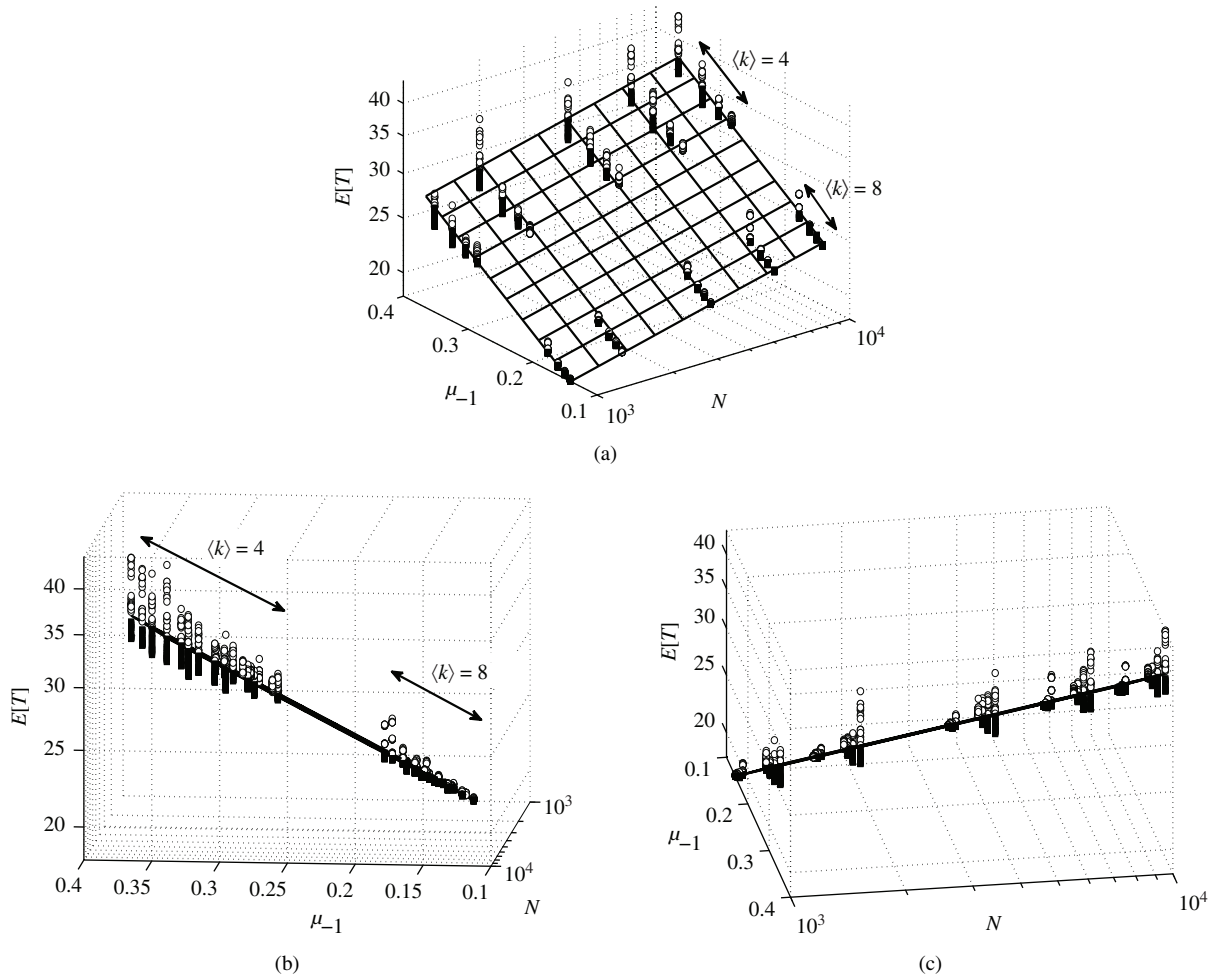


Fig. 8. (a) Takeover time ($E[T]$) as a function of the average inverse degree (μ_{-1}) and population size (N), for all scaling exponents (γ), assortativities (r), and average degrees ($\langle k \rangle$) considered in this paper. The data presented in (a) is also shown in (b) and (c), but from different viewing angles, in order to better elucidate the strength of the relationship between (b) $E[T]$ and μ_{-1} and (c) $E[T]$ and N . Note that in (a) and (b), $\langle k \rangle = 4$ corresponds to $m = 2$ and $\langle k \rangle = 8$ to $m = 4$. In (a)–(c), the plane represents the best fit to the data (see text); open circles denote data points above this plane and filled squares denote data below this plane. Note the logarithmic scaling of takeover time ($E[T]$) and population size (N) in each panel.

$\langle k \rangle = 4$, this causes the formation of long sections of linear chains of nodes [Fig. 2(b)]. In such topologies, placing the initial high-fitness genotype in a hub does not result in rapid saturation because its neighboring hubs are reluctant to adopt the high-fitness genetic information, as they too have many neighbors to choose from. Further, no matter where the initial high-fitness genotype is placed, this genetic information must still travel through the long chains of low-degree vertices, resulting in the lack of correlation between the degree of the vertex of initial placement and takeover time that was noted in [49].

Decreasing γ causes the interaction network to possess more highly connected vertices (e.g., for $N = 10\,000$, $k_{\max} = 27$ for $\gamma \sim 4.0$ and $k_{\max} = 140$ for $\gamma \sim 2.8$, Fig. 1). As previously discussed, in negatively assortative and uncorrelated topologies, such hubs communicate advantageous genetic information rapidly once they have it [46], [49], but their high connectivity makes them more resistant to it in the first place. This causes an increase in both the average takeover time and the variability in the takeover times observed on a single graph instance [Fig. 7]. In combination, high assortativity (r) and low

scaling exponents (γ) interact nonlinearly to increase takeover time [Fig. 3(b)].

Metrics based on pairwise shortest paths, such as characteristic path length (L), have a strong governing influence on the rate of information flow in many topologies. For example, expected takeover time ($E[T]$) is positively correlated with L in regular population structures [47]. However, the degree to which shortest path metrics govern information flow is dependent upon both network heterogeneity [49] and whether or not the local update mechanism is a function of vertex degree. Even if the update mechanism were independent of vertex degree, as in a *Susceptible-Infectious-Susceptible* model with 100% infection rate, L would still not be sufficient to describe the rate of spread in scale-free graphs, because the so-called characteristic path length is not actually characteristic of static structure in these graphs (as shown in Figs. 4 and 5). An alternative shortest path metric, the average maximum shortest distance from each vertex to any other vertex (i.e., the average eccentricity), will determine average saturation times when the update mechanism is independent of vertex degree, whether the graph is regular or not. However, when

the updating mechanism is degree-dependent and the graph is heterogeneous, shortest path metrics are not sufficient to describe dynamics.

Our results show that it is possible to describe the logarithm of the expected takeover time $E[T]$ using a planar function of: 1) the inverse average degree (μ_{-1}) and 2) the logarithm of population size $[\log_{10}(N)]$ [(12)]. Since the probability with which a vertex of degree k adopts the high fitness allele of a neighboring vertex is inversely proportional to k [(9)], it makes intuitive sense that the expected takeover time is a function of μ_{-1} , which weights the inverse degrees of the vertices in a graph in proportion to their occurrence [(3)] and thus captures the effects of both the average degree and the scaling exponent. Further, our observation that the logarithm of takeover time $[\log_{10}(E[T])]$ is linearly dependent on the logarithm of the population size $[\log_{10}(N)]$ has been noted in other studies of dynamical processes on scale-free graphs, including consensus time (i.e., the number of steps required to reach a state of all 0's or all 1's) in the unbiased Voter Model [42].

In [42], it was also shown that consensus times in the unbiased Voter Model on Molloy–Reed scale-free topologies [61] with a fixed average degree were largely governed by the effective population size, defined as $N_{\text{eff}} = N\mu_1^2/\mu_2$. However, this metric did not account for much of the variability in expected takeover times in our study. For the $\langle k \rangle = 4$ data, $R^2 = 0.64$ and for the $\langle k \rangle = 8$ data, $R^2 = 0.72$; however, the slopes and intercepts for these rather weak associations were quite different from each other, indicating a strong sensitivity of N_{eff} to average degree, so the overall R^2 was only 0.10. Although the two-state Voter Model (VM) used in [42] is similar in many ways to the takeover time study presented here, there are several significant differences in these models that can account for the differences in behavior. In the biased VM, state 0 is prescribed a fitness $f = 1$ and state 1 a fitness of $f = r$, with $r > 1$; in the unbiased case, there is no preference for either state, i.e., there is no selection pressure. In the VM, nodes are updated asynchronously, such that in each step a node i is chosen with probability inversely proportional to its fitness (in contrast to our implementation using locally uniform selection with synchronous updates). In the VM, node i then imports the state of a neighboring node j , irrespective of the fitness of node j (again, in contrast to our model which uses a replace-if-better update policy). Thus, the results of this paper complement those presented in [42], and highlight the sensitivity of information flow to the specific selection and update mechanisms. Future work will explore system responses to additional update mechanisms, such as the heterogeneous threshold-based update policies commonly used in models of binary decisions [32], in which the update rule of any given individual is contingent upon both the individual's particular response function and the states of its neighboring individuals.

Although the effects of assortativity were not explicitly studied in [42], the authors do comment that assortativity had a smaller secondary effect (relative to the scaling exponent) on consensus times. In this paper, we too found assortativity to have a secondary effect on mean takeover times. For example, (12), which does not account for the effects of assortativity, explains 97% of the variance in the

logarithmically transformed average takeover times. However, a closer examination of the data shows that, while assortativity has little effect on either mean or variability of average takeover times at the higher scaling exponents, at low scaling exponents assortativity has a pronounced effect on the variability in takeover times. Specifically, increasingly *positive* assortativities increased the variability between experiments on different random graph instances (after averaging over all initial placements on the same graph instance) [Fig. 9(a)], while increasingly *negative* assortativities increased the variability between takeover times from different initial placements on the same graph instances [Fig. 9(b)]. These seemingly contradictory findings can be explained as follows. At low scaling exponents (i.e., large hubs), the average system dynamics are sensitive to the specific connectivity patterns found in different graph instances with the same degree of positive assortativity, while the large number of very long individual path lengths (L_i) in these graphs means that they are relatively insensitive to initial placement of the high fitness individual, since these long paths must always be traversed. Conversely, at low scaling exponents with negative assortativity, all graph instances tend to have alternating high and low degree nodes and in this sense the connectivity patterns are relatively similar to each other, yet the takeover time is very sensitive to whether the initial high-fitness individual is placed in a high or low degree node, which respectively cause very short or long delays before the onset of the sigmoidal saturation process (Fig. 6). Thus, assortativity does have an important role in influencing systems dynamics on scale-free networks, especially if individual trajectories in specific systems are more relevant than average expected behaviors over an entire class of systems.

One of our goals has been to discover if there are simple, and easily computable, metrics of graph topology which govern the rate of spread of information in arbitrary networks. Previously, we have focused on metrics based on all-pairs shortest direct paths, such as characteristic path length, or a combination of the maximum and variance of the all-pairs shortest path lengths [47]. However, none of these has proven to govern system dynamics in the general case [49]. In this paper, we have also shown that neither the leading eigenvalue of the adjacency matrix nor the “effective population size” (N_{eff}) metric is sufficient to predict takeover times in these heterogeneous graphs. However, we did find that most of the variability in the logarithm of average takeover times in scale-free graphs with a wide range of scaling exponents, assortativities, number of nodes, and average node degree, can be explained by a function of the average inverse degree and the logarithm of the population size. Unfortunately, this relationship will not generalize to the case of regular graphs, in which the average inverse degree is constant for a given topology. For example, consider the contrasting cases of a lattice with Von Neumann neighborhoods ($\langle k \rangle = 4$) and a regular random graph of the same average degree. According to (12), the takeover times on these two topologies would be identical, while in reality the saturation times on a regular random graph will be much more rapid than those observed on the corresponding lattice with Von Neumann neighborhoods.

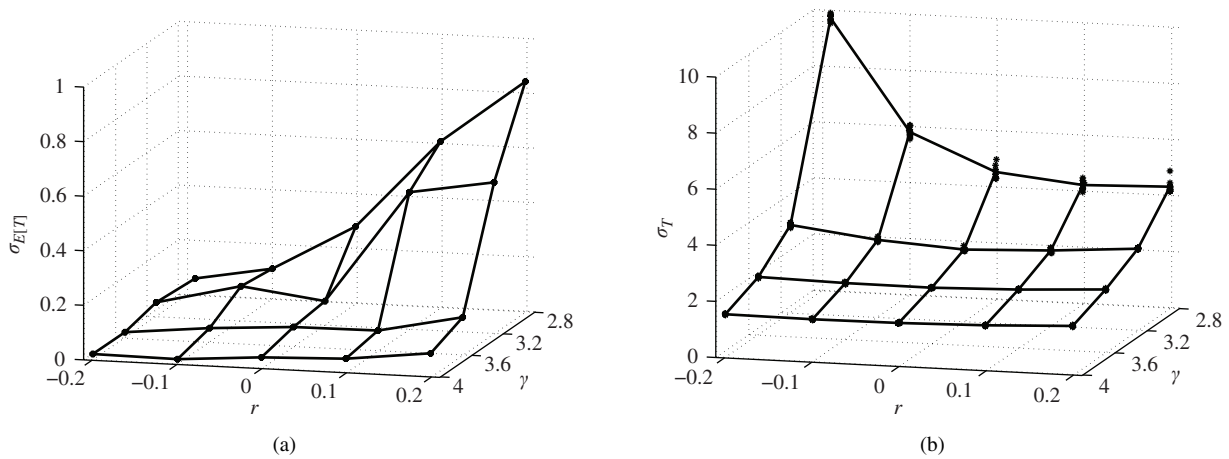


Fig. 9. (a) Standard deviation of expected takeover times ($\sigma_E[T]$) due to differences between the means on the ten graph instances at each parameter combination, and (b) Standard deviations of individual takeover times (σ_T) on the same graph instances, due to the N initial locations of the high fitness individual. In both (a) and (b), standard deviations are shown as a surface function of assortativity (r) and scaling (γ) at $N = 10\,000$, (k) = 4. Note that the scale of the vertical axis in (a) is an order of magnitude smaller than in (b).

The results of this paper demonstrate how the topological properties of randomized scale-free interaction networks influence the flow of advantageous alleles, and thus impact the selective pressures induced by such population structures. As previously mentioned, the few studies [35]–[38] that have utilized scale-free population structures for computational optimization have reported mixed results. However, to date all of the studies utilizing scale-free population structures for evolutionary optimization have employed graphs generated using the AB [26] algorithm, which exhibit no assortativity ($r \sim 0$) and have a scaling exponent that asymptotically approaches $\gamma = 3$. Thus, it remains unclear whether or not, and to what degree, the structural properties of the larger class of scale-free interaction networks (with variable scaling exponents and assortativity) can be exploited to improve the search performance of evolutionary algorithms, and how these topological characteristics relate to various aspects of problem difficulty, such as multimodality, epistasis, and deception. Since our results show that takeover times of individual experiments are highly sensitive to initial placement of the high fitness individual, especially at low scaling exponents in disassortative networks [Fig. 9(b)], we suspect that evolutionary algorithms on such networks would require multiple restarts to assure reliable results. However, the question as to whether the heterogeneity of these networks can sometimes lead to higher fitness solutions than on regular graphs remains to be seen. We have recently commenced further studies to try to address these questions.

The population structures utilized in evolutionary computation are typically static. That is, the interaction network is grown prior to the evolution of the population and it remains fixed throughout the evolutionary process. However, recent work has demonstrated that dynamic interaction network structures, both regular [62] and irregular [63], can enhance the search capabilities of population-based optimization algorithms. Specifically, Alba and Dorronsoro [62] showed that the solution quality of genetic algorithms can be improved by dynamically altering the dimensions of rectangular lattice

population structures, and Whitacre *et al.* [63] demonstrated that self-organizing complex interaction networks improve diversity maintenance in steady-state, asexual, mutation-limited populations. The results presented in this paper demonstrate that the selective pressures induced by scale-free interaction networks can be altered by changing the scaling exponent and/or assortativity, both of which can be achieved through edge swaps. Thus, it may be possible to dynamically alter the selective pressure in scale-free interaction networks, as an online means for controlling the exploration/exploitation tradeoff in evolutionary optimization.

The selection operators commonly used in evolutionary optimization may differ from the local uniform selection policy with replace-if-better updates employed in the bulk of this paper. However, experimentation with selection operators that are commonly employed in evolutionary optimization on regular population structures, such as binary tournament selection and linear ranking selection, produced qualitatively similar results to those observed using local uniform selection.

For each graph instance considered in this paper, care was taken to ensure that the edge sets were thoroughly randomized. We expect that scale-free interaction networks with more rigidly defined edge sets, such as the hierarchical and modular scale-free graphs considered in [30], [64], may induce qualitatively different selective pressures than those reported herein.

All of the experiments performed in this paper were nonextinctive, such that high-fitness individuals could not revert back to low fitness. Thus, the formulation of takeover time analysis considered herein implicitly assumed that once an advantageous mutation arose, it spread relentlessly. In evolutionary optimization, and other relevant contexts such as epidemiology, this is clearly a simplifying assumption; individuals with advantageous mutations are often lost before they are chosen for reproduction, and infectious individuals often recover before they spread disease. Thus, population structure influences the spread of genetic information by affecting: 1) the probability with which an advantageous mutation becomes

established and, once established, 2) the rate with which it spreads. While this paper investigated the latter influence of population structure, work is currently underway to investigate how the structural characteristics of scale-free interaction networks impact the former. As certain population structures are known to be promoters of the spread of advantageous alleles and others are known to be suppressors [65], [66], investigating the influence of the topological properties of scale-free interaction networks on establishment probabilities will complement the results presented in this paper.

In summary, in this paper we demonstrated why the so-called characteristic path length of a graph is not, in fact, characteristic of system dynamics on scale-free graphs with stochastic degree-dependent update mechanisms, because this metric does not account for variability in node degree. We also showed that the eigenvalues of the connectivity matrix and the effective population size (N_{eff}) are unable to account for observed variability in takeover times. Rather, we found that the logarithms of average takeover times on scale-free graphs, with a variety of scaling exponents, assortativities, and average degrees were well accounted for by a planar function of: 1) the average inverse degree (which incorporates the influence of scaling) and 2) the logarithm of the population size, and that there is a strong nonlinear effect of assortativity on the variability of takeover times at low scaling exponents. As the formulation of takeover time analysis considered herein serves as a simplified measure of information flow in general, we believe that the results of this paper may provide insights into a variety of dynamical processes which may occur on scale-free networks, such as epidemiological invasion, the dissemination of fads, ideas, and innovations, and evolutionary optimization.

APPENDIX

GLOSSARY OF VARIABLES

- 1) A_k : *Attachment kernel*—The attachment weight of a node of degree k , which is used to determine the probability ($\Pi(k)$) that an incoming node will attach to a node of degree k .
- 2) $E[T]$: *Expected takeover time*—Takeover time, averaged over all initial placements, on a single graph instance.
- 3) γ : *Scaling parameter*—The scaling exponent of a power-law degree distribution, $p(k) k^{-\gamma}$.
- 4) G : *Graph*—A graph $G = (V, E)$, comprised of a vertex set (V) and an edge set (E). In this paper, graph is used synonymously with *population structure*, *topology*, and *network*.
- 5) k : *Vertex degree*—The number of neighbors of a given node.
- 6) $\langle k \rangle$: *Average degree*—The average number of neighbors per node, which is equivalent to the first moment of the degree distribution (μ_1).
- 7) k_{\min} : *Minimum degree*—The minimum number of neighbors possessed by a node in a graph G .
- 8) k_{\max} : *Maximum degree*—The maximum number of neighbors possessed by a node in a graph G .
- 9) $\Lambda_i(t)$: *Vertex fitness*—The fitness of a vertex i at time t .

- 10) L_i : *Average individual path length*—Average shortest path between vertex i and all other vertices in a graph G .
- 11) L : *Characteristic path length*—Average all-pairs shortest distance between vertices.
- 12) μ_1 : *Average degree*—The first moment of the degree distribution, which is equivalent to the average degree ($\langle k \rangle$).
- 13) μ_{-1} : *Average inverse degree*—The first inverse moment of the degree distribution.
- 14) N : *Population size*—The number of vertices in a graph G .
- 15) N_{eff} : *Effective population size*—Defined in [42] as $N\mu_1^2/\mu_2^2$.
- 16) N_t : The proportion of high fitness nodes at time t .
- 17) $\Pi(k_i)$: The probability that a newly introduced vertex attaches to an existing vertex i of degree k_i .
- 18) $p(k)$: *Probability distribution function*—The probability of finding a node of degree k .
- 19) $P(k)$: *Complementary cumulative distribution function*—The probability of finding a node of degree greater than or equal to k .
- 20) P_{sel} : *Selection probability*—Probability of selecting a high fitness individual from a mating neighborhood.
- 21) r : *Assortativity*—Propensity of vertices of similar degree to attach to one another.
- 22) σ_T : Standard deviation of the takeover times observed in each individual graph instance (i.e., for each of the N initial placements of the high fitness individual, which are already averaged over the ten replicates of each initial placement).
- 23) $\sigma_{E[T]}$: Standard deviation of the expected takeover times across graph instances, for a given combination of γ , r , and N .
- 24) T : *Takeover time*—The takeover time observed in a single experiment.

ACKNOWLEDGMENTS

The authors thank P. Dodds, J. Bongard, G. Halnes, and B. Fath for helpful discussions. The computational resources provided by the Vermont Advanced Computing Center, which is supported by NASA (NNX 08A096G), are gratefully acknowledged.

REFERENCES

- [1] J. Werfel and Y. Bar-Yam, "The evolution of reproductive restraint through social communication," in *Proc. Nat. Academy Sci.*, vol. 101, no. 30, pp. 11019–11024, 2004.
- [2] M. A. Nowak and R. M. May, "Evolutionary games and spatial chaos," *Nature*, vol. 359, no. 6398, pp. 826–829, 1992.
- [3] C. Hauert and M. Doebeli, "Spatial structure often inhibits the evolution of cooperation in the snowdrift game," *Nature*, vol. 428, no. 6983, pp. 643–646, 2004.
- [4] F. C. Santos and J. M. Pacheco, "Scale-free networks provide a unifying framework for the emergence of cooperation," *Phys. Rev. Lett.*, vol. 95, no. 9, p. 098104, 2005.
- [5] H. Ohtsuki, C. Hauert, E. Lieberman, and M. A. Nowak, "A simple rule for the evolution of cooperation on graphs and social networks," *Nature*, vol. 441, no. 7092, pp. 502–505, 2006.
- [6] M. J. Eppstein and J. Molofsky, "Invasiveness in plant communities with feedbacks," *Ecol. Lett.*, vol. 10, no. 4, pp. 253–263, 2007.

- [7] M. J. Keeling, "The effects of local spatial structure on epidemiological invasions," *Proc. Royal Soc. London B: Biol. Sci.*, vol. 266, no. 1421, pp. 859–867, 1999.
- [8] R. Pastor-Satorras and A. Vespignani, "Epidemic spreading in scale-free networks," *Phys. Rev. Lett.*, vol. 86, no. 4, p. 3200, 2001.
- [9] M. E. J. Newman, "Spread of epidemic disease on networks," *Phys. Rev. E: Statist., Nonlinear, Soft Matter Phys.*, vol. 66, no. 1, p. 016128, 2002.
- [10] S. R. Borrett, B. D. Fath, and B. C. Patten, "Functional integration of ecological networks through pathway proliferation," *J. Theor. Biol.*, vol. 245, no. 1, pp. 98–111, 2007.
- [11] E. M. Rauch and Y. Bar-Yam, "Long-range interactions and evolutionary stability in predator-prey systems," *Phys. Rev. E: Statist., Nonlinear, Soft Matter Phys.*, vol. 73, no. 2, p. 020903, 2006.
- [12] B. Kerr, M. A. Riley, M. W. Feldman, and B. J. M. Bohannan, "Local dispersal promotes biodiversity in a real life game of rock-paper-scissors," *Nature*, vol. 418, no. 6894, pp. 171–174, 2002.
- [13] H. Sayama, L. Kaufman, and Y. Bar-Yam, "Spontaneous pattern formation and genetic diversity in habitats with irregular geographic features," *Conservation Biol.*, vol. 17, no. 3, pp. 893–900, 2003.
- [14] T. Reichenbach, M. Mobilia, and E. Frey, "Mobility promotes and jeopardizes biodiversity in rock-paper-scissors games," *Nature*, vol. 448, no. 7157, pp. 1046–1049, 2007.
- [15] L. Altenberg, "Evolvability suppression to stabilize far-sighted adaptations," *Artificial Life*, vol. 11, no. 4, pp. 427–443, 2005.
- [16] J. L. Payne and M. J. Eppstein, "Sensitivity of self-organized speciation to long-distance dispersal," in *Proc. IEEE Symp. Artificial Life*, 2007, pp. 1–7.
- [17] E. Alba and M. Tomassini, "Parallelism and evolutionary algorithms," *IEEE Trans. Evol. Comput.*, vol. 6, no. 5, pp. 443–462, Oct. 2002.
- [18] J. Lienig, "A parallel genetic algorithm for performance-driven VLSI routing," *IEEE Trans. Evol. Comput.*, vol. 1, no. 1, pp. 29–39, Apr. 1997.
- [19] F. Herrera and M. Lozano, "Gradual distributed real-coded genetic algorithms," *IEEE Trans. Evol. Comput.*, vol. 4, no. 1, pp. 43–63, Apr. 2000.
- [20] E. Cantú-Paz, "Markov chain models of parallel genetic algorithms," *IEEE Trans. Evol. Comput.*, vol. 4, no. 3, pp. 216–226, Sep. 2000.
- [21] G. Folino, C. Pizzuti, and G. Spezzano, "Parallel hybrid method for sat that couples genetic algorithms and local search," *IEEE Trans. Evol. Comput.*, vol. 5, no. 4, pp. 323–334, Aug. 2001.
- [22] G. Folino, C. Pizzuti, and G. Spezzano, "A scalable cellular implementation of parallel genetic programming," *IEEE Trans. Evol. Comput.*, vol. 7, no. 1, pp. 37–53, Feb. 2003.
- [23] D. A. Van Veldhuizen, J. B. Zydallis, and G. B. Lamont, "Considerations in engineering parallel multiobjective evolutionary algorithms," *IEEE Trans. Evol. Comput.*, vol. 7, no. 2, pp. 144–173, Apr. 2003.
- [24] M. Giacobini, M. Tomassini, A. Tettamanzi, and E. Alba, "Selection intensity in cellular evolutionary algorithms for regular lattices," *IEEE Trans. Evol. Comput.*, vol. 9, no. 5, pp. 489–505, Oct. 2005.
- [25] K. M. Bryden, D. Ashlock, S. Corns, and S. Wilson, "Graph based evolutionary algorithms," *IEEE Trans. Evol. Comput.*, vol. 10, no. 5, pp. 550–567, Oct. 2005.
- [26] A. L. Barabási and R. Albert, "Emergence of scaling in random networks," *Sci.*, vol. 286, no. 5439, pp. 509–512, 1999.
- [27] H. Ebel, L. Mielsch, and S. Bornholdt, "Scale-free topology of email networks," *Phys. Rev. E: Statist., Nonlinear, Soft Matter Phys.*, vol. 66, no. 3, p. 035103, 2002.
- [28] F. Liljeros, C. R. Edling, L. A. N. Amaral, H. E. Stanley, and Y. Aberg, "The web of human sexual contacts," *Nature*, vol. 411, no. 6840, pp. 907–908, 2001.
- [29] H. Jeong, B. Tombor, R. Albert, Z. N. Oltvai, and A. L. Barabási, "The large-scale organization of metabolic networks," *Nature*, vol. 407, no. 6804, pp. 651–654, 2000.
- [30] E. Ravasz, A. L. Somera, D. A. Mongru, Z. N. Oltvai, and A. L. Barabási, "Hierarchical organization of modularity in metabolic networks," *Sci.*, vol. 297, no. 5586, pp. 1551–1555, 2002.
- [31] H. Jeong, S. P. Mason, A. L. Barabási, and Z. N. Oltvai, "Lethality and centrality in protein networks," *Nature*, vol. 411, no. 6833, pp. 41–42, 2000.
- [32] D. J. Watts, "A simple model of global cascades on random networks," in *Proc. Nat. Academy Sci.*, vol. 99, no. 9, pp. 5766–5771, 2002.
- [33] J. Poncea, J. Gómez-Gardenes, L. M. Floría, and Y. Moreno, "Robustness of cooperation in the evolutionary prisoner's dilemma on complex networks," *New J. Phys.*, vol. 9, no. 6, p. 184, 2007.
- [34] Z. Rong, X. Li, and X. Wang, "Roles of mixing patterns in cooperation on a scale-free networked game," *Phys. Rev. E: Statist., Nonlinear, Soft Matter Phys.*, vol. 76, no. 2, p. 027101, 2007.
- [35] A. Gasparri, S. Panzieri, F. Pascucci, and G. Ulivi, "A spatially structured genetic algorithm over complex networks for mobile robot localisation," in *Proc. IEEE Int. Conf. Robot. Autom.*, Piscataway, NJ: IEEE Press, 2007, pp. 4277–4282.
- [36] M. Giacobini, M. Preuss, and M. Tomassini, "Effects of scale-free and small-world topologies on binary coded self-adaptive CEA," in *Proc. Evol. Comput. Combinatorial Optimization*, Heidelberg, Germany: Springer-Verlag, 2006, pp. 86–98.
- [37] M. Kirley and R. Stewart, "Multiobjective optimization on complex networks," in *Proc. 4th Int. Conf. Evol. Multicriterion Optimization (LNCS)*, 2007, pp. 81–95.
- [38] M. Kirley and R. Stewart, "An analysis of the effects of population structure on scalable multiobjective optimization problems," in *Proc. Genetic Evol. Comput. Conf. (GECCO '07)*, New York: ACM, pp. 845–852.
- [39] D. J. Watts and S. H. Strogatz, "Collective dynamics of small-world networks," *Nature*, vol. 393, no. 6684, pp. 440–442, 1998.
- [40] A. Clauset, C. R. Shalizi, and M. E. J. Newman, "Power-law distributions in empirical data," *arXiv:0706.1062v1*.
- [41] M. E. J. Newman, "Assortative mixing in networks," *Phys. Rev. Lett.*, vol. 89, no. 20, p. 208701, 2002.
- [42] V. Sood, T. Antal, and S. Redner, "Voter models on heterogeneous networks," *Phys. Rev. E: Statist., Nonlinear, Soft Matter Phys.*, vol. 77, no. 4, p. 041121, 2008.
- [43] D. Goldberg and K. Deb, "A comparative analysis of selection schemes used in genetic algorithms," in *Proc. Found. Genetic Algorithms*, San Francisco, CA: Morgan Kaufmann, 1991, pp. 69–93.
- [44] G. Rudolph, "On takeover times in spatially structured populations: Array and ring," in *Proc. 2nd Asia-Pacific Conf. Genetic Algorithms Applicat. (APGA '00)*, Hong Kong, China: Global Link Publishing Company, pp. 144–151.
- [45] J. Sarma and K. De Jong, "An analysis of the effect of neighborhood size and shape on local selection algorithms," in *Proc. Parallel Problem Solving from Nature*, Heidelberg, Germany: Springer-Verlag, 1996, pp. 236–244.
- [46] M. Giacobini, M. Tomassini, and A. Tettamanzi, "Takeover times curves in random and small-world structured populations," in *Proc. Genetic Evol. Comput. Conf. (GECCO '05)*, New York: ACM, pp. 1333–1340.
- [47] J. L. Payne and M. J. Eppstein, "Takeover times on scale-free topologies," in *Proc. Genetic Evol. Comput. Conf. (GECCO '07)*, New York: ACM, pp. 308–315.
- [48] P. Holme and B. J. Kim, "Growing scale-free networks with tunable clustering," *Phys. Rev. E: Statist., Nonlinear, Soft Matter Phys.*, vol. 65, no. 2, p. 026107, 2002.
- [49] J. L. Payne and M. J. Eppstein, "The influence of scaling and assortativity on takeover times in scale-free topologies," in *Proc. Genetic Evol. Comput. Conf. (GECCO '08)*, New York: ACM, pp. 241–248.
- [50] H. Caswell, *Matrix Population Models: Construction, Analysis, and Interpretation*. 2nd ed. Sunderland, U.K.: Sinauer Assoc., 2001, ch. 4, pp. 56–109.
- [51] J. L. Payne and M. J. Eppstein, "Pair approximations of takeover dynamics in regular population structures," *Evol. Comput.*, vol. 17, no. 2, pp. 203–229.
- [52] M. E. J. Newman, "The structure and function of complex networks," *SIAM Rev.*, vol. 45, no. 2, pp. 167–256, 2003.
- [53] M. Gorges-Schleuter, "An analysis of local selection in evolution strategies," in *Proc. Genetic Evol. Comput. Conf. (GECCO '99)*, San Francisco, CA: Morgan Kaufmann, pp. 847–854.
- [54] G. Caldarelli, A. Capocci, P. De Los Rios, and M. A. Munoz, "Scale-free networks from varying vertex intrinsic fitness," *Phys. Rev. Lett.*, vol. 89, no. 25, p. 258702, 2002.
- [55] K. Park, Y. C. Lai, and N. Ye, "Self-organized scale-free networks," *Phys. Rev. E: Statist., Nonlinear, Soft Matter Phys.*, vol. 72, no. 2, p. 026131, 2005.
- [56] V. D. P. Servedio, G. Calarelli, and P. Butta, "Vertex intrinsic fitness: How to produce arbitrary scale-free networks," *Phys. Rev. E: Statist., Nonlinear, Soft Matter Phys.*, vol. 70, no. 5, p. 056126, 2004.
- [57] P. L. Krapivsky, S. Redner, and F. Leyvraz, "Connectivity in growing random networks," *Phys. Rev. Lett.*, vol. 85, no. 21, p. 4629, 2000.
- [58] S. Maslov and K. Sneppen, "Specificity and stability in topology of protein networks," *Sci.*, vol. 296, no. 5569, pp. 910–913, 2002.
- [59] R. Xulvi-Brunet and I. M. Sokolov, "Reshuffling scale-free networks: From random to assortative," *Phys. Rev. E: Statist., Nonlinear, Soft Matter Phys.*, vol. 70, no. 6, p. 066102, 2004.
- [60] V. Batagelj and A. Mrvar, *Pajek-Program for Large Network Analysis* (1.24 ed.) [Online]. Available: <http://vlado.fmf.uni-lj.si/pub/networks/pajek/>

- [61] M. Molloy and B. Reed, "A critical point for random graphs with a given degree sequence," *Random Structures Algorithms*, vol. 6, no. 2, pp. 161–180, 1995.
- [62] E. Alba and B. Dorronsoro, "The exploration/exploitation tradeoff in dynamic cellular genetic algorithms," *IEEE Trans. Evol. Comput.*, vol. 9, no. 2, pp. 126–142, Apr. 2005.
- [63] J. M. Whitacre, R. A. Sarker, and Q. T. Pham, "The self-organization of interaction networks for nature-inspired optimization," *IEEE Trans. Evol. Comput.*, vol. 9, no. 2, pp. 157–170, Jun. 2008.
- [64] A. L. Barabási, E. Ravasz, and T. Vicsek, "Deterministic scale-free networks," *Physica A*, vol. 299, no. 3–4, pp. 559–564, 2001.
- [65] E. Lieberman, C. Hauert, and M. A. Nowak, "Evolutionary dynamics on graphs," *Nature*, vol. 433, no. 7023, pp. 312–316, 2001.
- [66] P. A. Whigham and G. Dick, "Evolutionary dynamics for the spatial moran process," *Genetic Programming Evolvable Mach.*, vol. 12, no. 2, pp. 220–230, 2008.



Margaret J. Eppstein received the B.S. degree in zoology from Michigan State University and the M.S. degree in computer science, Ph.D. degree in environmental engineering from the University of Vermont, Burlington.

She is currently an Associate Professor of Computer Science and Director of the Complex Systems Center, University of Vermont. Her current research interests include modeling and analysis of complex systems in a variety of application domains.



Joshua L. Payne (S'04) received the B.S. degree in mathematics and computer science from Regis University, Denver, CO, the M.Eng. degree in operations research and statistics from Rensselaer Polytechnic Institute, Troy, NY, and is currently working toward the Ph.D. degree in computer science at the University of Vermont, Burlington. His dissertation is entitled "Interaction Topologies and Information Flow."